Progress In Electromagnetics Research C, Vol. 11, 155–170, 2009

RADIATION FROM CAVITY-BACKED FRACTAL APERTURE ANTENNAS

B. Ghosh, S. N. Sinha, and M. V. Kartikeyan

Department of Electronics and Computer Engineering
Indian Institute of Technology Roorkee
Roorkee 247667, India

Abstract—This paper investigates the properties of probe fed cavity-backed fractal aperture antennas. The problem is formulated using the finite element-boundary integral (FE-BI) method in which the field inside the cavity is formulated using the finite element method, and the mesh is truncated at cavity aperture surface using the boundary integral method. Several dual-band cavity-backed fractal aperture antennas based on Sierpinski gasket, Sierpinski carpet, plus shape fractal and Minkowski fractal are investigated. The numerical results obtained from the FE-BI code have been validated with simulations on HFSS.

1. INTRODUCTION

Slot antennas form an important class of antennas which are preferred in applications where low-profile, flush-mounted, and conformal antennas are required. One shortcoming of slot antennas is their bi-directional radiation characteristic which is alleviated by using a shallow cavity on one side of the slot. The performance of several cavity-backed aperture antennas has been investigated in the past [1–4]. With the recent trends in the design of compact communication systems, a demand has arisen for antennas which can be operated in multiple frequency bands. This has led to the use of fractal geometries whose self-similarity property has been exploited in the design of a number of multi-band printed antennas. Recently, some fractal printed slot antennas have also been investigated using Koch fractal [5], circular fractal slot [6], and Sierpinski curves [7]. In this paper, we investigate the radiation properties of some typical fractal slot antennas backed by a cavity.

Corresponding author: B. Ghosh (basugdec@iitr.ernet.in).

The finite element-boundary integral (FE-BI) method has been used to analyze the problem, since it is an efficient and versatile numerical technique for the analysis of cavity-backed aperture antennas [8]. The technique employs the finite element method to compute the electromagnetic field inside the cavity and the cavity volume mesh is terminated at the aperture surface using boundary integral method [9]. The method generates a partly sparse and partly filled matrix which can be efficiently stored and solved. In the absence of suitable fabrication facilities, simulation on HFSS has been used to validate the results obtained from FE-BI analysis.

The article is organized as follows: A general formulation of radiation from cavity-backed aperture antennas using the finite element-boundary integral method is presented in Section 2. In Section 3, numerical results of different cavity-backed fractal aperture antennas are presented. Section 4 summarizes the results.

2. FORMULATION OF THE PROBLEM

A typical coaxial probe-fed cavity-backed aperture antenna is shown in Fig. 1, where the apertures can be of arbitrary shape and number. The antenna is fed by a coaxial probe of inner radius ρ_1 and outer radius ρ_2 and is located at (x_c, y_c). The problem is formulated using the FE-BI method using tetrahedral elements for cavity discretization. The open region above the cavity top surface is truncated using boundary integral (BI) method and the aperture surface at the bottom of the cavity is formulated using eigenfunction expansion method. By combining these three methods, the entire problem can be transformed into a linear system.

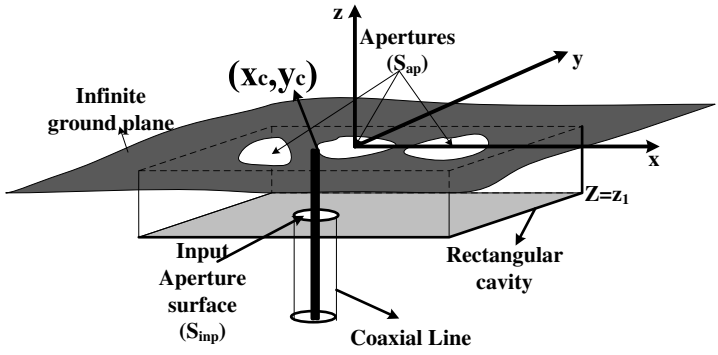

Figure 1. Geometry of a coaxial probe-fed cavity backed aperture antenna.

For a linear, isotropic and source free region, the electric field satisfies the vector wave equation given by

$$\nabla \times \left(\frac{1}{\mu_r} \nabla \times \bar{E} \right) - k_0^2 \varepsilon_r \bar{E} = 0 \tag{1}$$

where μ_r and ε_r are, respectively, the permeability and permittivity of the medium inside the cavity.

Multiplying (1) scalarly by a testing function $\bar{T}$ and integrating over the volume of the cavity, we get

$$\iiint_V \bar{T} \cdot \nabla \times \left(\frac{1}{\mu_r} \nabla \times \bar{E} \right) dv - k_o^2 \varepsilon_r \iiint_V \bar{T} \cdot \bar{E} dv = 0 \tag{2}$$

where V denotes the volume of the cavity.

Using vector identities, the above expression can be written as

$$\iiint_V \frac{1}{\mu_r} \left(\nabla \times \bar{T} \right) \cdot \left(\nabla \times \bar{E} \right) dv - k_0^2 \varepsilon_r \iiint_V \bar{T} \cdot \bar{E} dv = j\omega\mu_0 \oiint_S (\bar{T} \times \hat{n}) \cdot \bar{H} ds \tag{3}$$

where $\hat{n}$ is the unit outward normal to cavity surface S.

The tangential component of the electric field is zero on the perfectly conducting walls of the cavity, except on the aperture surfaces. Thus, the surface integral on the right hand side of (3) is non zero only over the aperture surfaces (S_{ap}) on the infinite ground plane and on the input aperture surface (S_{inp}) on the cavity bottom. Therefore, (3) can be rewritten as,

$$\begin{aligned} &\iiint_V \frac{1}{\mu_r} (\nabla \times \bar{T}) \cdot (\nabla \times \bar{E}) dv - k_0^2 \varepsilon_r \iiint_V \bar{T} \cdot \bar{E} \; dv \\ &- j\omega\mu_0 \iint_{S_{ap}} (\bar{T} \times \hat{n}) \cdot \bar{H}_{ap} ds = j\omega\mu_0 \iint_{S_{inp}} (\bar{T} \times \hat{n}) \cdot \bar{H}_{inp} ds \end{aligned} \tag{4}$$

where, $\bar{H}_{ap}$ and $\bar{H}_{inp}$ denote the magnetic fields on the aperture surfaces S_{ap} and S_{inp}, respectively.

Thus, the problem can be divided into three parts. The first part involves the computation of volume integrals inside the cavity volume. The second and third parts involve the evaluation of surface integrals over the apertures on the top surface of the cavity and the input aperture surface, respectively. The cavity is first discretized into small tetrahedral elements and over each tetrahedral element, vector edge basis functions [10] are defined. The surface integral over the aperture surface on the top surface of the cavity is calculated using the equivalence principle and the magnetic field in the open space region is calculated by considering an equivalent magnetic surface current $2\bar{M}$, where $\bar{M} = \bar{E} \times \hat{z}$, radiating in free space. The surface integral over the

input surface at the bottom of cavity is computed by expanding the electric field as the sum of incident and reflected fields. The procedure is same as that described in [11]. The combination of these three integrals can be expressed is matrix form as

$$A(k)e(k) = b(k) \tag{5}$$

where $b(k)$ is the excitation vector, $e(k)$ denotes the coefficient vector and $A(k)$ is a partly sparse and partly dense matrix which is a combination of three matrices and may be written as

$$A(k) = A_1(k) + A_2(k) + A_3(k) \tag{6}$$

with

$$A_1(k) = \iiint_V \frac{1}{\mu_r}(\nabla \times \bar{T}) \cdot (\nabla \times \bar{E})dv - k_0^2 \varepsilon_r \iiint_V \bar{T} \cdot \bar{E} dv \tag{7}$$

$$A_2(k) = jk_0 Z_0 \iint_{S_{ap}} \bar{T}_s \cdot \bar{H}_{ap}(2\bar{M})ds \tag{8}$$

$$A_3(k) = \frac{jk_0\sqrt{\varepsilon_{rc}}}{2\pi \ln\left(\frac{\rho_2}{\rho_1}\right)} \left\{ \iint_{S_{inp}} \left(\bar{T} \cdot \frac{\hat{\rho}}{\rho}\right) ds \iint_{S_{inp}} \left(\bar{E} \cdot \frac{\hat{\rho}}{\rho}\right) ds \right\} \tag{9}$$

$$b(k) = \frac{2jk_0\sqrt{\varepsilon_{rc}}}{\sqrt{2\pi \ln\left(\frac{\rho_2}{\rho_1}\right)}} \iint_{S_{inp}} \bar{T} \cdot \left(\frac{\hat{\rho}}{\rho}\right) ds \tag{10}$$

where ε_{rc} is the permittivity of material inside coaxial line.

Once the matrix equation (5) is solved for the unknown coefficients, the field over the aperture surface can be calculated. The input reflection coefficient at the incident plane ($z_1 = 0$) is then given by [11]

$$\Gamma = \frac{1}{\sqrt{2\pi \ln\left(\frac{\rho_2}{\rho_1}\right)}} \iint_{S_{inp}} \bar{E} \cdot \frac{\hat{\rho}}{\rho} ds - 1 \tag{11}$$

The magnetic field in the far-field region can be calculated as

$$\bar{H}(r, \theta, \varphi) = -\frac{jk_0}{\eta_0} \frac{e^{-jk_0 r}}{2\pi r} \iint_{S_{ap}} (\hat{\theta}\hat{\theta} + \hat{\varphi}\hat{\varphi}) \cdot \bar{M} e^{jk_0 \sin\theta(x\cos\varphi + y\sin\varphi)} dxdy \tag{12}$$

3. NUMERICAL RESULTS

Based on the formulation presented here, a MATLAB code has been developed to analyze the performance of cavity-backed fractal aperture

antennas. Several fractal aperture antennas have been investigated and the results are presented in the following subsections. For the aperture antennas considered here, the dimension of the cavity is taken to be $15\,\text{cm} \times 15\,\text{cm} \times 0.4\,\text{cm}$ and the cavity is assumed to be fed by a coaxial probe of $50\,\Omega$ characteristic impedance.

3.1. Sierpinski Carpet Fractal Aperture

The generation of Sierpinski carpet fractal aperture is described in [12], where an initial square is subdivided into nine subsquares and the central subsquare is removed to obtain the generator of the fractal. The self-similarity factor of the Sierpinski carpet is 3 which causes a log-periodic behavior with a periodicity of 3. To have control over the location of resonant frequencies, the fractal geometry is modified as shown in Fig. 2. Here, we have used a rectangle as the initial geometry. The length of the first iteration aperture is one third of the initial length of the rectangle and in the second iteration, the length of the second iteration apertures is varied according to scale factor (s). For the present analysis, the dimension of the initial rectangle is taken to be $15\,\text{cm} \times 7.5\,\text{cm}$. Hence, in the first iteration, the antenna consists of a single aperture of length 5 cm and width 2.5 cm. In the second iteration, the dimensions of the apertures are $4\,\text{cm} \times 0.83\,\text{cm}$ with a scale factor (s) equal to 0.8.

First, a parametric study is performed for the optimum position of the probe and from the study, it is found that the optimum positions of the probe are at (0, 6.0 cm) and (0, 5.4 cm) for 1st and 2nd iterations, respectively. The frequency response of the antenna is shown in Fig. 3, where a good agreement between the FE-BI code and HFSS results can be seen. The frequency response of the aperture antenna for two iterations is tabulated in Table 1. It is seen that the first resonant frequency shifts slightly downwards in second iteration and the ratio between the successive resonant frequencies is 1.39 which is slightly

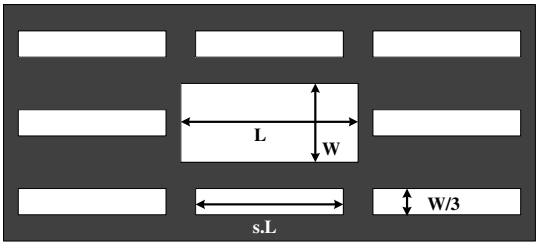

Figure 2. A modified 2nd iteration Sierpinski carpet fractal aperture.

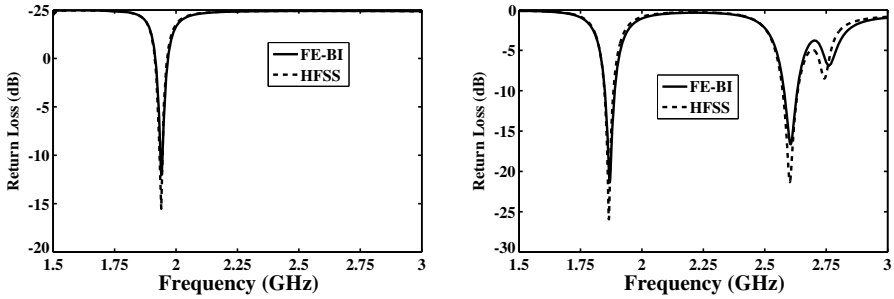

Figure 3. Return loss of modified Sierpinski carpet fractal aperture antenna with $s = 0.8$.

Table 1. Frequency response of modified Sierpinski carpet fractal aperture antenna.

Parameters	Iteration 1	Iteration 2	
	f_{r1}	f_{r1}	f_{r2}
Resonant Freq. (GHz)	1.94	1.87	2.60
VSWR	1.25	1.09	1.32
Bandwidth (%)	1.55	1.98	2.50

Table 2. Frequency response of modified Sierpinski carpet fractal aperture antenna for different scale factors.

Scale Factor	Resonant Frequencies		Ratio	Bandwidth (%)	
(s)	f_{r1}	f_{r2}	f_{r2}/f_{r1}	BW_1	BW_2
0.7	1.89	2.74	1.45	1.85	1.83
0.8	1.87	2.60	1.39	1.98	2.50
0.9	1.82	2.36	1.30	2.31	2.58

greater than the theoretical ratio of 1.25. The ratio between the successive resonant frequencies can be controlled by changing the scale factor (s). Two more fractal structures with different scale factors were analyzed. The variation of return loss of the antenna for different scale factors is shown in Fig. 4 and the results are summarized in Table 2.

The optimum probe location for the two antennas with $s = 0.7$ and $s = 0.9$ are $(0, 5.7\,\text{cm})$ and $(0, 5.0\,\text{cm})$, respectively. It is evident that while the first resonant frequency is relatively insensitive to the

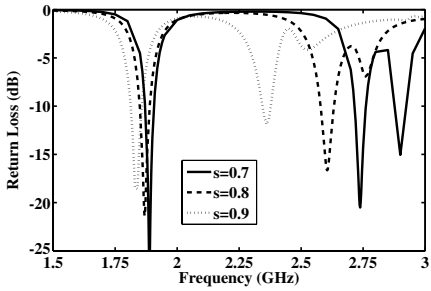

Figure 4. Return loss of modified Sierpinski carpet fractal aperture antenna for different scale factors.

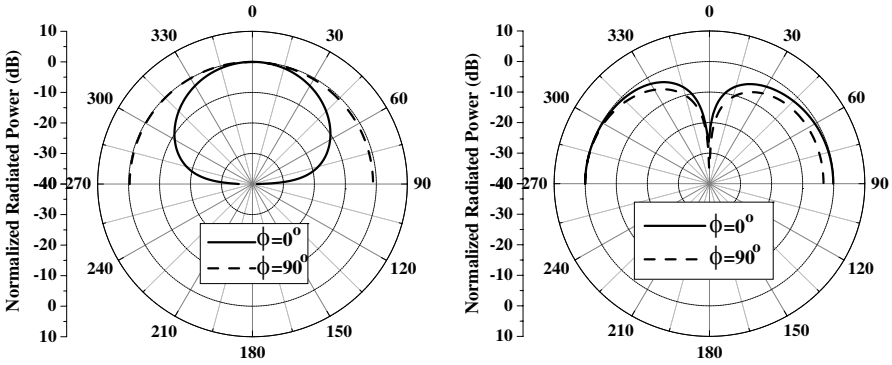

(a) 1st Resonance (b) 2nd Resonance

Figure 5. Normalized radiation pattern of modified Sierpinski carpet fractal aperture antenna with $s = 0.8$.

variation in scale factor and is primarily dependent on the size of initial rectangle; the second resonant frequency can be suitably located by selecting an appropriate scale factor. The frequency ratios are greater than the theoretical value which is a characteristic of the pre-fractal geometries for lower order iterations. Also, the ratios between the successive resonant frequencies depend on the position of slot relative to the center of the cavity and the location of resonant frequencies can be fine tuned by varying the spacing between the apertures.

The normalized radiation pattern of a 2nd iteration modified Sierpinski carpet aperture in the two principal planes is shown in Fig. 5 for $s = 0.8$. At the second resonant frequency (2.6 GHz), the cavity is excited in TM_{120} mode which has a field pattern such that the second iteration apertures are excited in opposite phase, causing a null to appear along z-axis.

3.2. Self-affine Sierpinski Gasket Dipole Apertures

The generation of Sierpinski gasket dipole geometry is same as that of the Sierpinski gasket fractal except that an image of the original structure is taken along the base line of the initial triangle. In order to maintain the continuity of the apertures, a certain amount of overlapping is incorporated and the final geometry of the 2nd iteration self-affine Sierpinski gasket dipole aperture with a scale factor $s = 0.8$ is shown in Fig. 6. From the parametric analysis, it was found that the optimum position of the probe was at $(0, 5.25\,\text{cm})$ for both iterations. The variation of return loss of the fractal aperture antenna for two iterations is shown in Fig. 7 and the results are tabulated in Table 3. Again a good agreement between the results from FE-BI code and those obtained from HFSS simulation can be seen for both iterations. It can be seen that there is a 8.05% downward shift of first resonant

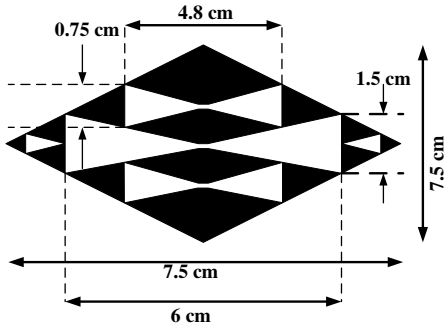

Figure 6. A modified 2nd iteration Sierpinski gasket dipole fractal aperture.

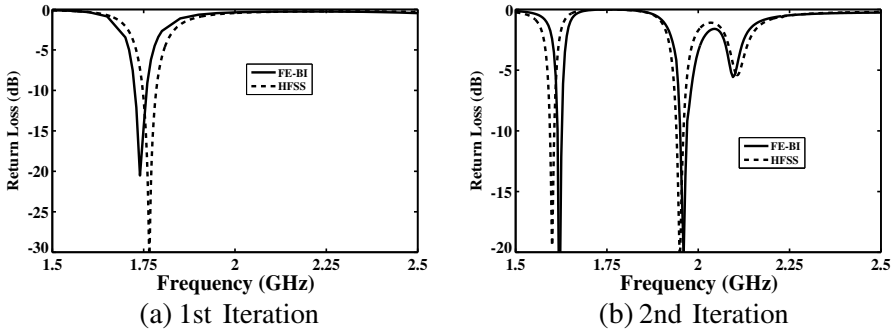

Figure 7. Return loss of modified Sierpinski gasket dipole fractal aperture antenna with $s = 0.8$.

Table 3. Frequency response of modified Sierpinski gasket dipole fractal aperture antenna.

Parameters	Iteration 1	Iteration 2	
	f_{r1}	f_{r1}	f_{r2}
Resonant Freq. (GHz)	1.74	1.60	1.95
VSWR	1.10	1.09	1.12
Bandwidth (%)	2.15	0.75	1.03

frequency in the second iteration. The ratio between the successive resonant frequencies is 1.22, which is slightly less than the theoretical value 1.25. The bandwidth of the antenna decreases as the order of iteration increases. Although the input match is good in all the iterations, the bandwidth of the antenna is very small at both the resonant frequencies. In order to see the effect of scale factor on the response of the antenna, another gasket dipole aperture antenna with a scale factor $s = 0.6$ was investigated. The dimensions of the first iteration aperture were kept constant at 6 cm, so the length of the 2nd iteration aperture was 3.6 cm. The variation of return loss of 2nd iteration self-affine gasket dipole aperture antenna for different scale factors is shown in Fig. 8. It can be seen that there is a very little change in the first resonant frequency and the location of the 2nd resonance can be controlled by changing the scale factor. The resonant frequencies for $s = 0.6$ are 1.58 GHz and 2.38 GHz with a ratio of 1.49. This ratio is much less than the theoretical ratio of 1.67. This is due to the geometric modifications incorporated in the generation of fractal aperture. Also, it is well known that for a rectangular aperture antenna, the resonant aperture length approaches 0.5λ as the resonant frequency of the antenna moves closer to the fundamental resonant mode of the closed cavity [13]. However, as the resonant frequencies move away from fundamental resonant mode, the ratio decreases, which is another reason of smaller frequency ratio for $s = 0.6$.

The normalized radiation pattern of the 2nd iteration gasket dipole aperture antenna with $s = 0.8$ is shown in Fig. 9 in two principal planes and is similar at both resonant frequencies. The maximum gain of the aperture antenna at the resonant frequencies is around 4 dB. It is to be noted here that both the resonant frequencies for the dipole aperture antenna are within the fundamental resonant mode of the closed cavity, hence, the pattern at both resonant frequencies remains same.

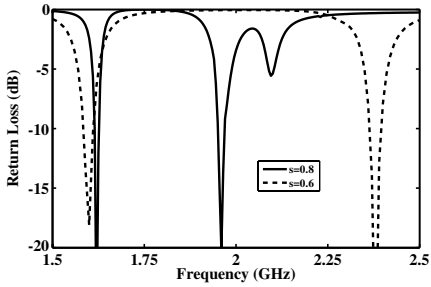

Figure 8. Return loss of modified Sierpinski gasket dipole fractal aperture antenna for different scale factors.

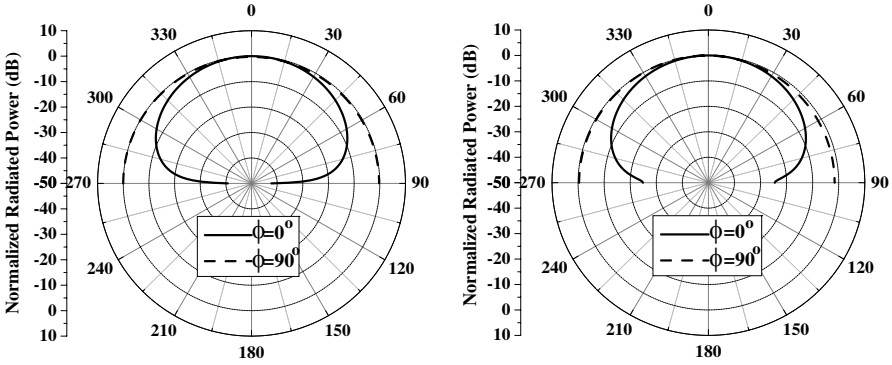

(a) 1st Resonance (b) 2nd Resonance

Figure 9. Normalized radiation pattern of modified Sierpinski gasket dipole fractal aperture antenna with $s = 0.8$.

3.3. Self-affine Plus Shape Fractal Aperture Antenna

Plus shape fractal apertures are widely used in the design of frequency selective surfaces [14]. An ideal plus shape fractal is generated by placing four copies of initial geometry, each of which is scaled by 0.5. Here, we have considered a self-affine plus shape fractal aperture upto second iteration only. The initial plus shape has a horizontal arm length L and vertical arm length W and the width of each arm is taken to be Ws. The initial geometry is scaled by a factor s in both directions and four such copies are placed with an offset (d_x, d_y) as shown in Fig. 10. In the present analysis, the initial plus shape is assumed to have a length $L = W = 5\,\text{cm}$ and the width of each arm is 2 mm. The variation of return loss for first iteration plus fractal aperture antenna

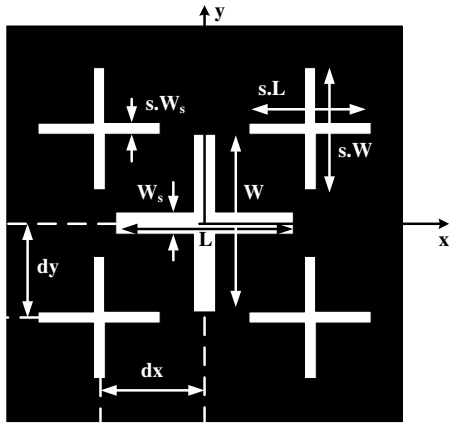

Figure 10. A self-affine 2nd iteration plus shape fractal aperture antenna.

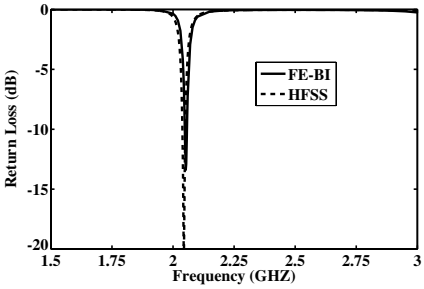

Figure 11. Return loss of 1st iteration plus shape fractal aperture antenna.

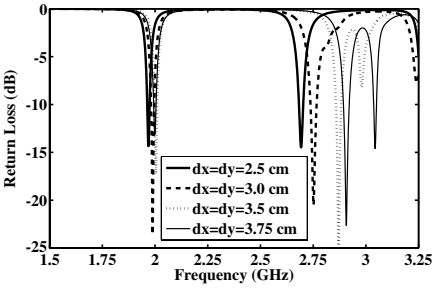

Figure 12. Return loss of 2nd iteration plus shape fractal aperture antenna for different offset values.

with probe at (0, 6.5 cm) is shown in Fig. 11. Also shown in the figure are the results obtained from HFSS which are in good agreement with the FE-BI analysis. The initial plus aperture antenna resonates at 2.05 GHz with a 10-dB bandwidth of 0.45%. Next, a 2nd iteration plus shape aperture antenna was investigated for different values of offset parameters (d_x, d_y) with a scale factor of $s = 0.8$. Fig. 12 shows the variation of return loss for different offset values and the results are summarized in Table 4. It is evident that the location of the 2nd iteration aperture affects the location of 2nd resonant frequency and hence, the ratio of successive resonant frequencies. The variation of return loss for a 2nd iteration aperture with $d_x = d_y = 2.5$ cm is shown in Fig. 13. It is seen that the first resonant frequency shifts downward

Table 4. Frequency response of 2nd iteration plus shape fractal aperture antenna for different offset values.

Offset ($d_x = d_y$)	x_c (cm)	y_c (cm)	Resonant Frequencies		Ratio
			f_1 (GHz)	f_2 (GHz)	f_2/f_1
2.50	0	6.6	1.97	2.69	1.37
3.00	0	6.4	1.99	2.75	1.38
3.50	0	6.4	2.00	2.87	1.44
3.75	0	6.25	2.00	2.91	1.46

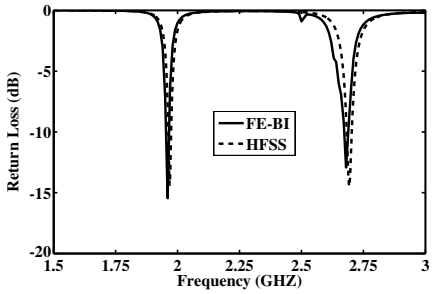

Figure 13. Return loss of 2nd iteration plus shape fractal aperture antenna with $d_x = d_y = 2.5\,\text{cm}$ and $s = 0.8$.

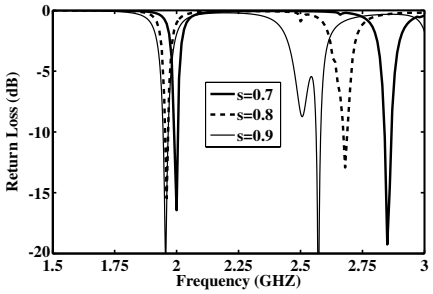

Figure 14. Return loss of 2nd iteration plus shape fractal aperture for different scale factors.

and the ratio between the successive resonant frequencies is 1.36 as compared to the theoretical value 1.25. Two more plus shape fractal apertures with scale factors $s = 0.7$ and $s = 0.9$ were investigated and the results are shown in Fig. 14. The value of offset was kept at 2.5 cm. It is seen that the ratio between the successive resonant frequencies are 1.425, 1.37 and 1.31 for $s = 0.7$, $s = 0.8$ and $s = 0.9$, respectively. Thus, the antenna resonant frequency can be controlled by changing the scale factor, which can be fine tuned with different offset values.

The radiation pattern of the 2nd iteration plus shape fractal aperture antenna is shown in Fig. 15. The pattern shows a similar behavior as that of carpet antenna which shows a null along z-axis.

3.4. Minkowski Fractal Aperture Antenna

Minkowski fractal geometries are widely used in the miniaturization of antenna and frequency selective surface design. Here, we have considered a second iteration Minkowski aperture antenna. The

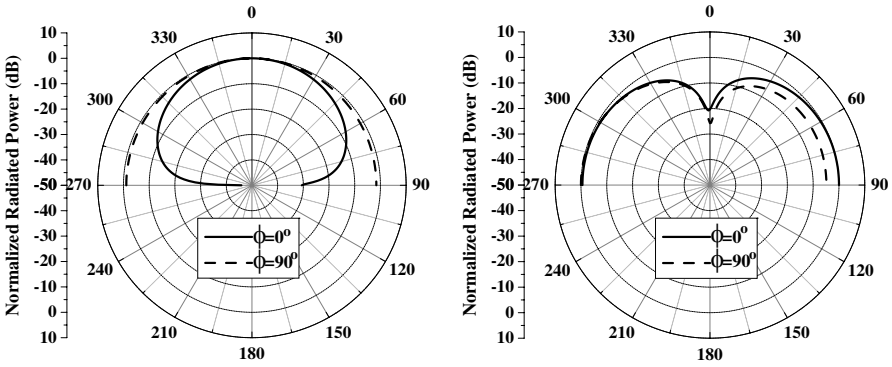

(a) 1st Resonance (b) 2nd Resonance

Figure 15. Normalized radiation pattern of self affine 2nd iteration plus shape fractal aperture antenna with $s = 0.8$.

dimension of the initial square is taken to be 3 cm × 3 cm and a 10 cm × 10 cm × 0.4 cm cavity is used. The geometry of the Minkowski aperture is shown in Fig. 16. From the parametric analysis, it was found that the optimum probe locations are (0, 4.25 cm), (0, 3.80 cm) and (0, 3.60 cm) for three iterations, respectively. The frequency response of the Minkowski fractal aperture for different iterations of the fractal geometry is shown in Fig. 17. It is found that the resonant frequency of the antenna decreases by 12.66% as the order of iteration increases from 0th to 2nd iteration. The ratio of the square aperture length to the resonant wavelength is 0.31. Generally, it is found that the antenna bandwidth decreases with the miniaturization of the antenna structure. However, in this case, the antenna bandwidth increases as the order of iteration increases and the impedance match for all the iterations is very good.

The normalized power patterns of 2nd iteration Minkowski aperture antenna at the resonant frequency are shown in Fig. 18. Although not shown in the figure, the power patterns at the resonant frequencies of the aperture antenna for different iterations were studied and it was found that the pattern remains same at the resonant frequencies for all iterations, although the gain of the antenna decreases with the increase in order of iteration. The maximum gains of the antenna at the resonant frequencies for different iterations are 6.76 dB, 5.88 dB and 5.45 dB.

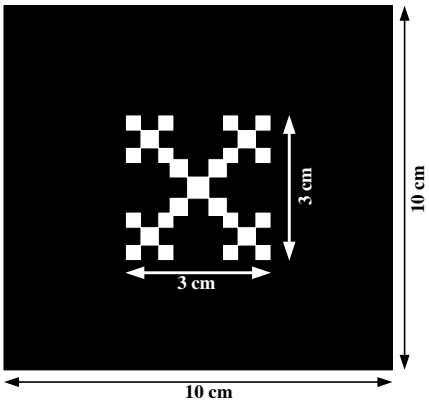

Figure 16. A 2nd iteration Minkowski fractal aperture antenna.

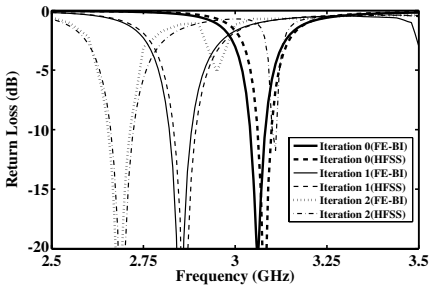

Figure 17. Return loss of Minkowski fractal aperture antenna for different iterations.

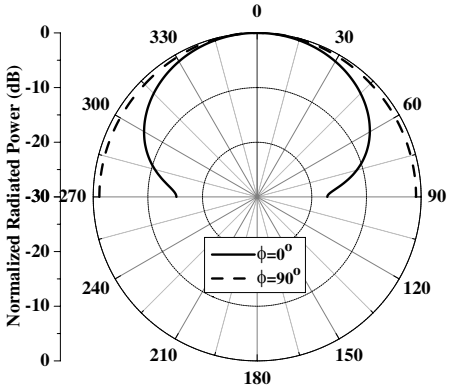

Figure 18. Normalized radiation pattern of 2nd iteration Minkowski aperture antenna.

4. CONCLUSIONS

A hybrid FE-BI analysis for the cavity backed aperture antenna with a coaxial feed is presented. Some dual-band cavity-backed antennas based upon self-affine fractal geometries, such as, Sierpinski gasket, Sierpinski carpet, plus shape fractal and Minkowski fractal have been investigated and discussed. It is observed that the scale factor of the fractal apertures can be used to suitably locate the resonant frequencies of the antenna. Also, it is found that the location of the aperture

relative to the center of the cavity changes the frequency characteristics of the antenna. One of the main drawbacks of the cavity backed antenna is that they have a low bandwidth which is due to the cavity resonances. The normalized radiation pattern of the antenna is the same at both the resonant frequencies for Sierpinski gasket dipole aperture antenna, but a null appears along z-axis for aperture antennas like Sierpinski carpet and plus shape fractal antennas. From the results presented here, it can be concluded that the radiation pattern of the antenna can be kept same if the apertures are excited by a single cavity mode. A self-similar antenna based on the Minkowski fractal is also analyzed, and it is found that this fractal geometry can be useful to minimize the dimension of aperture antenna.

REFERENCES

1. Shi, S., K. Hirasawa, and Z. N. Chen, "Circularly polarized rectangularly bent slot antennas backed by a rectangular cavity," *IEEE Trans. Antennas Propagat.*, Vol. 49, 1517–1524, Nov. 2001.
2. Takahashi, T., T. Kotani, K. Hirasawa, and S. Shi, "A rectangular cavity-backed cross-loop slot antenna," *Proc. IEEE Int. Symp. Antennas Propagat.*, 448–451, Mar. 2002.
3. Kotani, T., K. Hirasawa, and S. Song, "A rectangular cavity-backed S-type slot antenna," *Proc. IEEE Int. Symp. Antennas Propagat.*, Vol. 4, 490–493, Jun. 2003.
4. Takahashi, T. and K. Hirasawa, "A broadband rectangular cavity backed meandering slot antenna," *Proc. IEEE Int. Workshop Antenna Technol.: Small Antennas and Novel Metamaterials*, 21–24, Mar. 2005.
5. Sundaram, A., M. Maddela, and R. Ramadoss, "Koch-fractal folded-slot antenna characteristics," *IEEE Antennas Wireless Propagat. Lett.*, Vol. 6, 219–222, 2007.
6. Chang, D., B. Zeng, and J. Liu, "CPW-fed circular fractal slot antenna design for dual-band applications," *IEEE Trans. Antennas Propagat.*, Vol. 56, 3630–3636, Dec. 2008.
7. Hu, R., J. Li, and S. Fan, "A novel fractal folded-slot antenna using Sierpinski curves," *Proc. IEEE Int. Conf. Communication Systems*, 371–373, Nov. 2008.
8. Jin, J. M. and J. L. Volakis, "A hybrid finite element method for scattering and radiation by microstrip patch antennas and arrays residing in a cavity," *IEEE Trans. Antennas Propagat.*, Vol. 39, 1598–1604, Nov. 1991.

9. Jin, J. M., *The Finite Element Method in Electromagnetics*, John Wiley and Sons, New York, 2002.
10. Chatterjee, A., J. M. Jin, and J. L. Volakis, "Computation of cavity resonances using edge-based finite elements," *IEEE Trans. Microw. Theory Tech.*, Vol. 40, 2106–2108, Nov. 1992.
11. Reddy, C. J., M. D. Deshpande, C. R. Cockrell, and F. B. Beck, "Analysis of three dimensional cavity-backed aperture antennas using combined finite element method/method of moment/ geometrical theory of diffraction technique," NASA Technical Paper 3548, Hampton, Verginia, Nov. 1995.
12. Peitgen, H. O., H. Jurgens, and D. Saupe, *Chaos and Fractal: New Frontiers of Science*, Springer-Verlag, New York, 1992.
13. Chang, T. N., L. C. Kuo, and M. L. Chuang, "Coaxial-fed cavity backed slot antenna," *Microw. Opt. Technol. Lett.*, Vol. 14, 291–294, Apr. 1997.
14. Gianvittorio, J. P., J. Romeu, S. Blanch, and Y. Rahmat-Samii, "Self-similar prefractal frequency selective surfaces for multiband and dual-polarized applications," *IEEE Trans. Antennas Propagat.*, Vol. 51, 3088–3096, Nov. 2003.